Mol. Cryst. Liq. Cryst., Vol. 604: pp. 71–83, 2014

ISSN: 1542-1406 print/1563-5287 online
DOI: 10.1080/15421406.2014.968030

Properties of Electrodeposited WO_3 Thin Films

JULIANA R. DE ANDRADE,[1] IVANA CESARINO,[1]
RUI ZHANG,[2] JERZY KANICKI,[2]
AND AGNIESZKA PAWLICKA[1,2,*]

[1]IQSC-USP, São Carlos-SP, Brazil
[2]Department of Electrical Engineering and Computer Science, University of Michigan, Ann Arbor, MI, USA

Galvanostatic electrodeposition was used to produce transparent and amorphous WO_3 films that showed color changes from clear to blue in response to the applied potential of ±1.0 V. The 61% in transmittance variation was measured at wavelength of 633 nm. The roughness of 16.7 nm was obtained by atomic force microscopy (AFM). The scanning electron microscopy (SEM) evidenced homogeneous morphology without cracks but with some regularly disposed spots attributed to the nucleation sites. The SEM images also confirmed the thicknesses of 143 nm. The electro-optic data analysis gave the coloration efficiency value of 11.6 cm^2/C. Finally, the electrical measurements evidenced an existence of the negative capacitance.

Keywords WO_3; electrodeposition; negative capacitance

1. Introduction

Tungsten trioxide (WO_3) thin film is widely studied electrochromic material due to its reversible color change [1, 2]. Such film can be prepared by different vacuum or wet deposition methods [2] and used in different electrochemical devices such as electrochromic windows [3, 4], energy storage devices [5] and chemical sensors [6, 7]. The WO_3 as catalysts was also investigated in the last 40 years [8, 9].

Among many thin films deposition technologies the sol-gel methods appear to be very interesting when compared with expensive vacuum techniques [10]. It is low cost approach such as dip-coating, spray-coating or roll-coating methods that could allow to produce a large area coatings. Among many reports on different sol-gel techniques only a few describe on electrodeposition of amorphous electrochromic tungsten trioxide (WO_3) thin films [11–13].

In present work we describe the results of the galvanostatically deposited WO_3 thin films with improved electro-optical properties when compared to potenciostatically deposited films [12].

*Address correspondence to Agnieszka Pawlicka, IQSC-USP, Av. Trabalhador Sãocarlense 400, 13566-590 São Carlos-SP, Brazil. E-mail: agnieszka@iqsc.usp.br

Color versions of one or more of the figures in the article can be found online at www.tandfonline.com/gmcl.

2. Experimental

2.1 Electrodeposition of WO_3

0.5 mol/L solution for WO_3 electrochemical deposition was obtained by dissolution of 6.5 g of tungsten metal powder (Fmaia) in the mixture of 15 ml of H_2O_2 (30%, Synth), 15 mL of acetic acid and 15 mL of ethanol at 0°C under magnetic stirring and reflux for 3 days. Next, the solution was filtered and the resulting peroxotungstic acid powder dried using rotary evaporator. The yellow fine powder was then dissolved in 75 mL of absolute ethanol and the clear pale yellow plating sol with $1 \leq \text{pH} \leq 2$ was stored in the refrigerator [14].

Galvanostatic electrodeposition was performed in a three electrode electrochemical cell with a platinum plate as the auxiliary electrode, an indium-tin-oxide (ITO) coated glass substrate (Delta Technologies CD-50IN-1505; 5–15 Ω/□; 1 cm × 3 cm × 0.5 mm) as the working electrode and the reference electrode being Ag/AgCl/KCl. Prior to film deposition, the substrates were cleaned with acetone, absolute ethanol, Extran (Aldrich) and Milli-Q® water. The electrodeposition was performed by applying a constant current of −0.45 mA for 10 min at room temperature [15]. The resulting 143 nm thick transparent films were then annealed at 120°C in air for 1h and stored in vacuum desiccator.

2.2 Microstructure Characterization

The structure of the films was examined by X-ray diffraction measurements using Rigaku Rotaflex model RU200B instrument with CuKα radiation ($\lambda = 1.542$ Å) and a scattering angle range of $2\theta = 5$ to 60° with a speed of 1°/min and step of 0.02.

Scanning electron microscope (SEM) images were obtained by Hitachi SU8010 and LEO 440 with EDX analyzer. The sample was cut by ADT 7100 dicing saw as part of preparation of acquiring cross section SEM image.

The atomic force microscopy (AFM) images were obtained with Nanosurf easy Scan 2 AFM System in the contact mode by using silicon AFM probes with a force constant of 0.2 N/m and the resonance frequency of 13 kHz.

2.3 Electrochemical Characterization

Cyclic voltammetry (CV) and chronocoulometry analysis using Autolab PGSTAT 302N were performed in a classical three-electrode electrochemical cell within ±1.0 V; WO_3 thin film was a working electrode, Ag was a reference electrode and a Pt plate was an auxiliary electrode. The electrolyte was 0.1M $LiClO_4$ in propylene carbonate (PC).

2.4 Optical Measurements

The optical transmittance in UV-Vis range spectra were recorded with an Agilent 8452A spectrophotometer between 190 and 1100 nm at room temperature in air. The electrodeposited and annealed WO_3 thin films were placed in special three-electrode electrochemical cell with two quartz windows as showed in Fig. 1. WO_3 thin film was a working electrode, Ag wire was a reference electrode and a Pt plate was an auxiliary electrode. The electrolyte was 0.1 mol/L $LiClO_4$ in propylene carbonate (PC).

Figure 1. Three-electrode electrochemical cell with two quartz windows and WO_3 blue colored thin film inside the cell.

2.5 Electrical Measurements

The electrical and dielectric characterization measurements were carried out with Aglient B1500A analyzer, HP 4284A LCR meter and Alessi probe station. Current density (J)- voltage (V) characteristic was measured by using ITO/WO_3/Mo structure on glass substrate. One probe was contacted to top Mo layer and the other one to bottom ITO layer (as shown in Fig. 9 inset), where Mo layer was deposited by DC sputtering with a thickness of 108 nm and ITO film was 74 nm thick. Capacitance (C) - voltage (V) characteristics were measured by using same structure at frequencies of 10 kHz, 100 kHz and 1MHz respectively. P+ c-Si/SiO_2/Mo metal-insulator-semiconductor (MIS) and Mo/SiO_2/Mo metal-insulator-metal (MIM) devices were also measured as references, where silicon oxide thin films were prepared by plasma-enhanced chemical vapor deposition (PECVD) using Plasmatherm PECVD tool. In addition, as deposited ITO/WO_3/Mo structure was exposed to water vapor for 1 minute to investigate the moisture effect on its capacitance characteristic change. The exposed sample was cooled down and dried in N_2 gas flow for 5 minutes before dielectric measurements.

3. Results and Discussion

3.1 Electrochemical Properties of WO_3

Fig. 2 shows the results of galvanostatic electrodeposition of WO_3 thin film, for 600 s, at a current of -0.45 mA. It is possible to see that the value of potential drops abruptly in the first few seconds, demonstrating the reduction of peroxytungstic acid species that are near the working ITO electrode. In the case of cathodically deposited tungsten trioxide films the reduction of peroxy-tungstate determined a film growth with good approximation [13]. At the remaining time, the tendency of stabilization of potential is observed, that can be explained by the control of the electrodeposition by diffusion, similarly to the Prussian Blue film deposition [16].

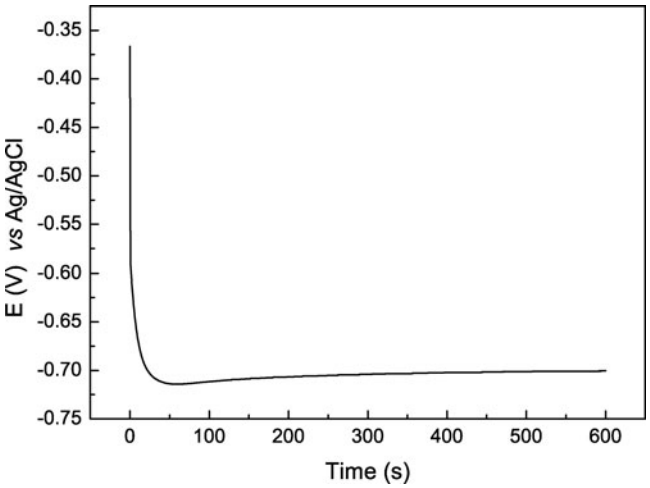

Figure 2. Electrodeposition curve of WO_3 film at -0.45 mA for 600 s.

The cyclic voltammograms for the WO_3 films annealed at 120°C, depicted in Fig. 3 and recorded at different scan speeds of 50, 100, 200, 300 and 500 mV/s, were obtained by sweeping the potential in the range of -1.0 to $+1.0$ V vs. Ag in 0.1 mol/L $LiClO_4$/PC. From this figure one can observe an increase of the cathodic current density to -1.0 mA/cm^2 at -1.0 V, due to the reduction process occurring in the film and consequently its switch to the blue color; at -0.25 V for the scan rate of 50 mV/s anodic peak is observed and is due to the oxidation process and bleaching of the film [17]. Similarly to the results reported by Deepa et al. [18] an increase of the voltammetric scan rate promotes an increase of the cathodic current density to -2.0 mA/cm^2 and also the shifts of the anodic peak to more positive potentials of 0 V at 500 mV/s.

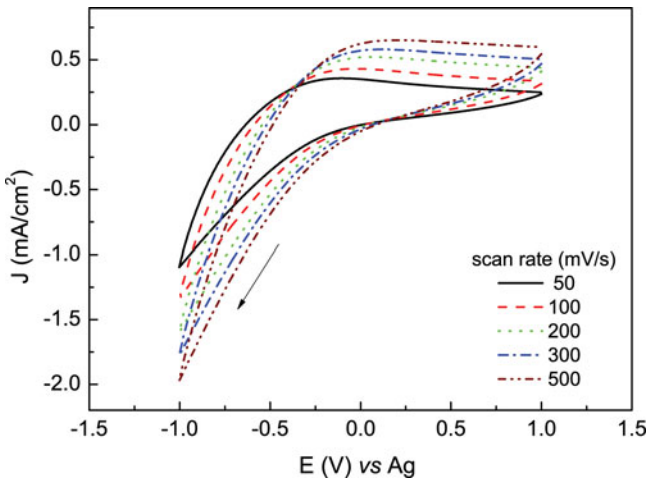

Figure 3. Cyclic voltammograms of the electrodeposited WO_3 thin film, recorded at different scan speeds of 50, 100, 200, 300 and 500 mV/s. The arrow indicates the scan direction.

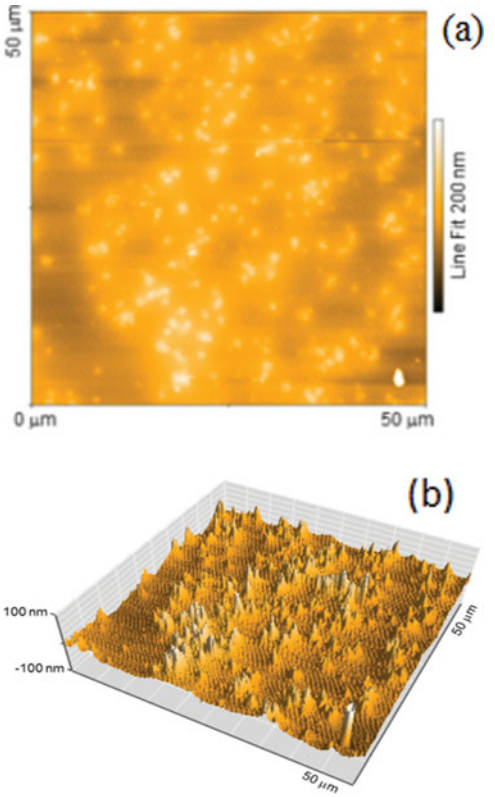

Figure 4. AFM images of electrodeposited WO_3 thin film; top (a) and side (b) view.

The electrochemical redox stability of the films, evaluated by chronoculommetry ($\pm$1.5 V for 15 s/15 s) is evidenced by a decrease in the ion-charge capacities of -33 mC/cm^2 measured for 5th cycle to 30 mC/cm^2 after 3,000th cycles (not shown here). This result is similar to the results reported by Orel et al. [19].

3.2 Structural Properties of WO_3

Aiming to investigate the morphology of the deposited films atomic force microscopy (AFM) was used. As a comparison the ITO surface (not shown here) was also analyzed evidencing flat and smooth morphology with root mean square (RMS) roughness of 4.9 nm. Contrary to ITO, WO_3 thin film on ITO substrate displays a very rough topology (Fig. 4) with the RMS roughness of 16.7 nm. Moreover, as shown on the Fig. 4a some uniformly distributes white spots are also observed. Comparing this figure with Fig. 4b it can be stated that these spots are the tops of the hills formed during the WO_3 deposition with average height of 34.2 $\pm$ 10.2 nm and the average length of 0.96 $\pm$ 0.28 nm. The presence of these hills can be due to the nuclei formation, in the initial stage of electrodeposition as also observed on the SEM image (Fig. 5c).

Aiming to analyze the morphological characteristics of these thin films scanning electron microscopy was used for visualization of the coating surface. Fig. 5 shows SEM micrographs of electrodeposited WO_3 thin films annealed at 120°C, where one can observe

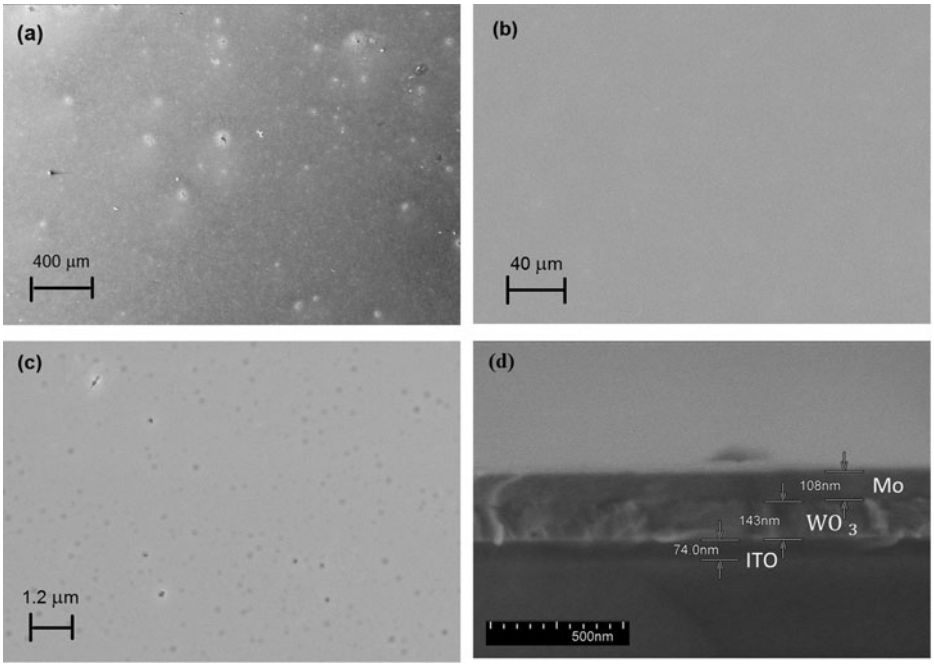

Figure 5. SEM images of galvanostatic deposited WO_3 films at 100× (a), 1,000× (b) and 20,000× (c) and cross section of glass/ITO/WO_3/Mo structure (d).

almost good homogeneity without cracks. However, the picture of 100× magnification (Fig. 5a) reveals some lighter spots, which can be attributed to the agglomerates formation and/or impurities adsorbed during the film deposition. These spots can be also due to the no complete peroxytungstic acid dissolution. Amplification to 1,000× (Fig. 5b) of some regions of the WO_3 film surface, reveals to be very uniform, however. Higher amplification to 20,000× (Fig. 5c) again reveals some uniformly distributes spots of about 150–200 nm of diameter, which can be due to the nucleation points formed on the beginning of the electrodeposition, as already observed by AFM analysis (Fig. 4). Fig. 5d shows a cross section of glass/ITO/WO_3/Mo structure, where a thickness of 143 nm of an electro-deposited tungsten trioxide thin film can be confirmed. The WO_3 coatings obtained in present work are thinner than reported by Munro et al. [14] for the dip-coated 200–400 nm thick films and by Kalagi et al. [20] for the sputtered films. Moreover, these coatings evidenced also a DRX amorphous structure (not shown here) [21, 22].

3.3 Optical and Spectroelectrochemical Properties of WO_3

In situ spectroelectrochemical studies show the change of the film color when voltage is applied. The colored and bleached and/or reduced and oxidized, respectively states of the WO_3 films are shown in Fig. 6. As can be seen in this figure electrodeposited WO_3 thin film samples exhibit transparency of ∼70% in the visible range (Fig. 6 – inset a). The application of negative potential (−1.0 V) promotes the color change to blue (Fig. 6 – inset b) and a drop of transmittance of the film to less than 10% at the same time. At 633 nm the change in transmittance level between transparent and blue-colored states of the WO_3 film is equal to 61% [23].

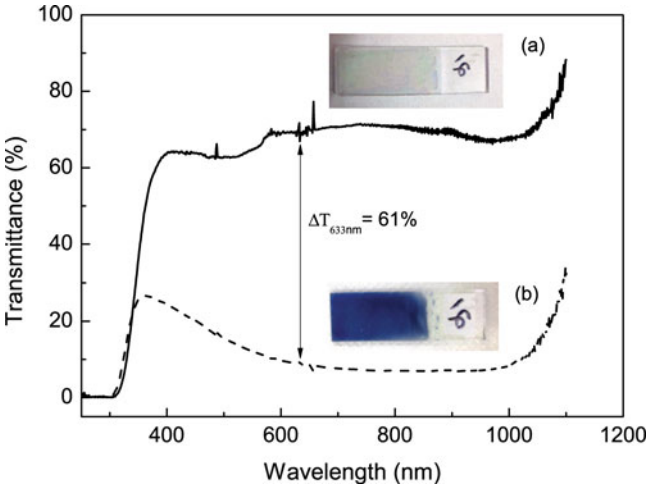

Figure 6. UV-Vis *in situ* of WO_3 thin film in the colored (——) and bleached (- - - -) states after E = −1.0 V and E = +1.0 V applications, respectively. Pictures of bleached (inset a) and colored film (inset b) are also shown.

The tungsten trioxide network can accommodate cations such as H^+, Li^+, etc., is undergoing a reversible intervalence transition reaction and the color change, as follows [2]:

$$WO_3(transparent) + xM^+ + xe^- \leftrightarrow M_xWO_3(blue\ colored)(M = H^+, Li^+, Na^+ etc)$$

Furthermore, the color/bleaching kinetics of the films, was studied by *in situ* absorbance changes at $\lambda = 633$ nm during 15 s cathodic (−1.0 V) and 15 s anodic (+1.0 V) charge insertion and extraction (Fig. 7a), respectively as a function of time during last 30 of 3,000 cycles performed (Fig. 7b). Results reveal very stable behavior, where the absorbance changes of 0.58 for E = ± 1 V, i.e., from 0.2 for transparent to 0.78 for blue color thin film. From this experiment it can be stated that neither coloring nor bleaching processes are affected by the repetitive color/bleaching cycling suggesting good electrochemical reversibility of the WO_3 thin film prepared by electrodeposition method.

To investigate in more detail the electrodeposited electrochromic thin film opto-electrochemical properties the absorbance difference (ΔOD) was plotted against inserted charge (Q_{ins}; measured with Autolab PGSTAT 302N). Optical density values for the applied potentials of −0.9 to −1.5 V are displayed in Fig. 8, where one can observe a linear dependence of ΔOD on inserted charge. Furthermore, it was possible to calculate the coloration efficiency of $\eta = 11.6$ cm^2/C, through the formula (1) [2],

$$\eta = \frac{\Delta OD}{Q_{ins}} \tag{1}$$

The η value obtained in this work is lower when compared to the value of 118 cm^2/C, obtained for WO_3 annealed at 250°C [11] and of 60 cm^2/C for the sputtered thin films reported by Lee et al. [24]. The obtained coloration efficiency is almost the same when compared to the values of 12.6 cm^2/C for the film annealed at 100°C and 16.3 cm^2/C for the film annealed at 250°C [12].

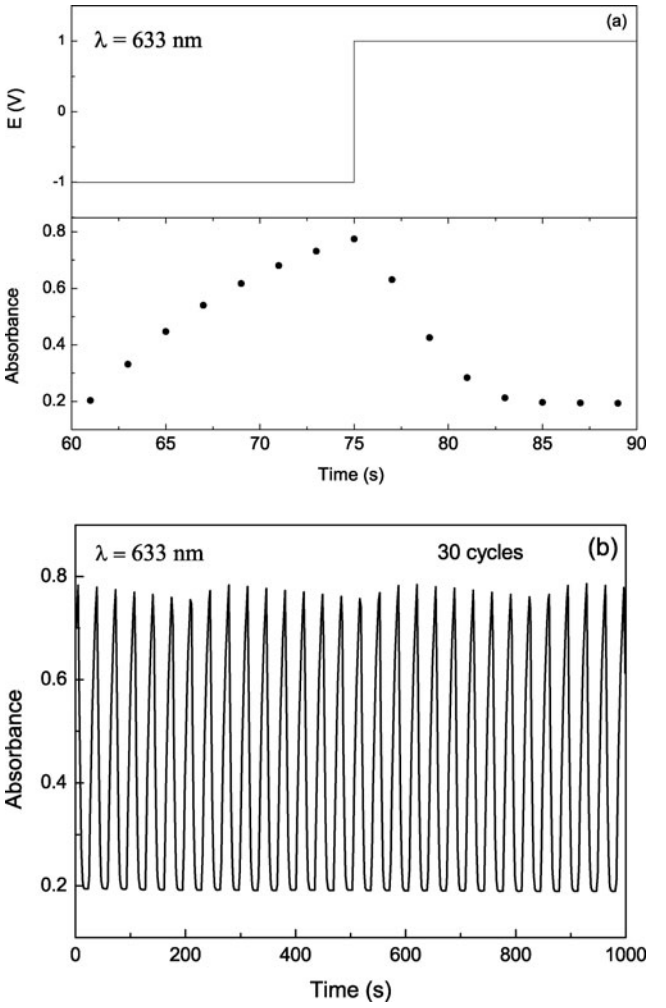

Figure 7. Insertion and extraction cycles of *in situ* absorbance–time response of WO_3 film at $\lambda = 633$ nm on the application of potential (E) of ± 1.0 V (15s/15s) (a). Last 30 cycles of *in situ* absorbance–time response of WO_3 film on the application of potential of ± 1.0 V (15s/15s) for 3,000 cycles (b).

3.4 Electrical Properties of WO_3

Electro-deposited WO_3 thin films were also characterized by electrical and dielectric measurements. Fig. 9 shows measured current density (J)- voltage (V) characteristic of electrodeposited tungsten trioxide thin film in both logarithmic (continuous line to right) and linear (dashed line to left) scales. Form this figure it can be observed that J-V curve increases above applied voltage of $+5$ V. This increase is nearly linear with the applied voltage. No critical breakdown is observed for this material. We can also observe that current continuously increases once voltage is applied. For these observations we can conclude that further optimization will be needed to use this material as gate insulator.

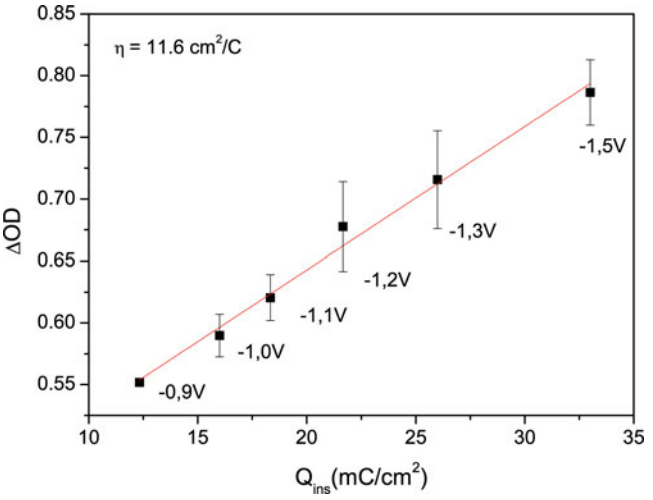

Figure 8. ΔOD as a function of inserted charge for the WO_3 thin films annealed at 120°C and measured at $\lambda = 633$ nm for applied potentials of -0.9 to -1.5 V.

Fig. 10 shows measured capacitance density (C)- voltage (V) characteristics of electro-deposited tungsten trioxide thin film, where all results were normalized. From the C-V curve, it is clearly observed a negative capacitance values in range of applied voltage from -5 to 5 V and there is no significant difference between responses when voltage is applied from 0 to -5 V or from 0 to $+5$ V, which is consistent with Granqvist et al. [25] observation on nanocrystalline WO_3 films. Negative capacitance were observed at all measured frequencies, including 10 kHz, 100 kHz, and 1 MHz, where a common negative value of around -1.5 μF/cm^2 was measured at all frequencies near 0 V. When applied voltage increases (or decreases) from 0 V, measured negative capacitance drops, where the

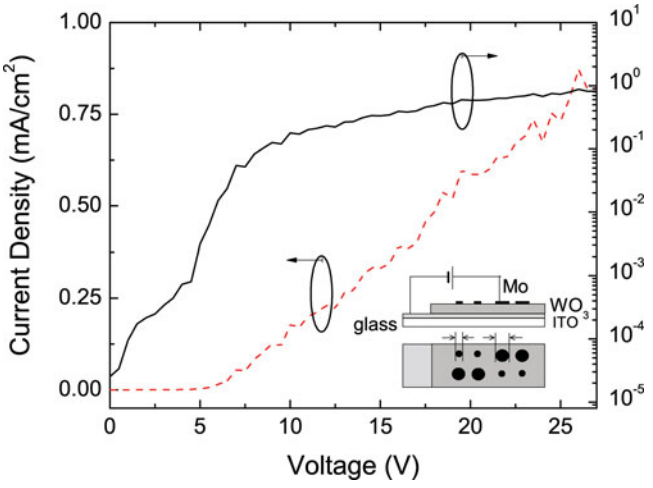

Figure 9. Current density (J)- voltage (V) characteristic of electro-deposited tungsten trioxide film measured by using ITO/WO_3/Mo structure (as shown in inset).

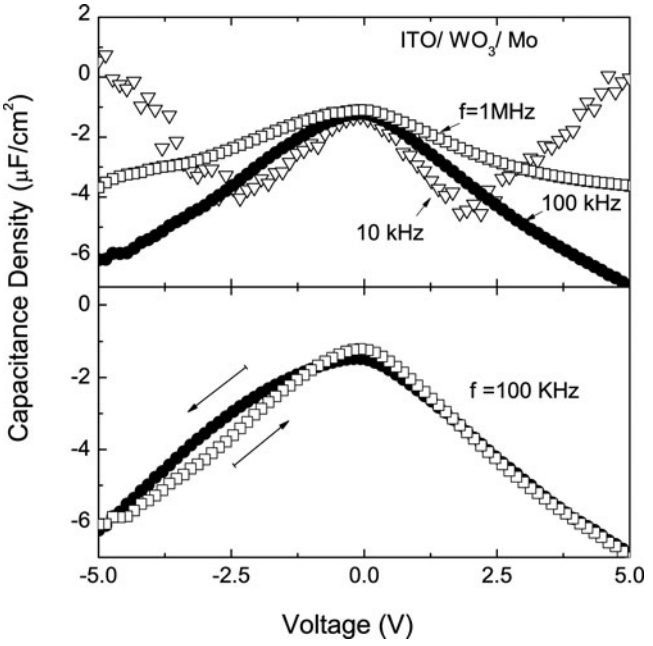

Figure 10. Capacitance density (C)- voltage (V) characteristic of electro-deposited WO_3 films measured using ITO/WO_3/Mo structure: (top) C-V measured at 10 kHz, 100 kHz and 1 MHz; (bottom) C-V measured with applied voltage starts from -5 to $+5$ V and from $+5$ to -5 V, respectively.

C-V results look like reverse quadratic curves, at 100 kHz and 1 MHz. C-V curve measured at 10 kHz, however, displays a unique W-shape, where valleys exited at ± 2.5 V and capacitance value breaks through zero near ± 5 V. C-V characteristics were also measured at 100 kHz with applied voltage starting from -5 to $+5$ V and from $+5$ to -5 V. Two overlapped C-V curves, shown in Fig. 10, indicate that there is no significant hysteresis.

To make sure that the measured negative capacitance is real we also measured C-V characteristic of the silicon dioxide (SiO_2) as reference sample. Fig. 11 shows C-V characteristics of referenced silicon dioxide thin films measured using both Mo/SiO_2/Mo and Mo/SiO_2/p+c-Si structures. Both C-V curves show normal as expected behavior consistent with Ceiler et al. [26] previous report. It has also been proved that the observed negative capacitance characteristic of electrodeposited WO_3 thin film is convincible. In addition Fig. 11 shows the change in C-V characteristic when WO_3 is exposed to water vapor. We can see decrease in capacitance value after water vapor exposure for 1 min. This result indicates that the negative capacitance characteristic of electrodeposited WO_3 film is associated with the water adsorption by WO_3.

To explain this result two possible explanations can be proposed: (*i*) H_2O, which has a dielectric constant of 40$\sim$80, penetrate into WO_3 film and fill in the voids existed in the films. The influence of water on electrochemical properties and its penetration in the CeO_2-TiO_2 thin films were already observed [27]. Consequently the presence of water in the WO_3 coating changes the total film capacitance by series/parallel connection of the capacitance associated with water (C_{H_2O}) and capacitance associated with WO_3 (C_{WO_3}) as

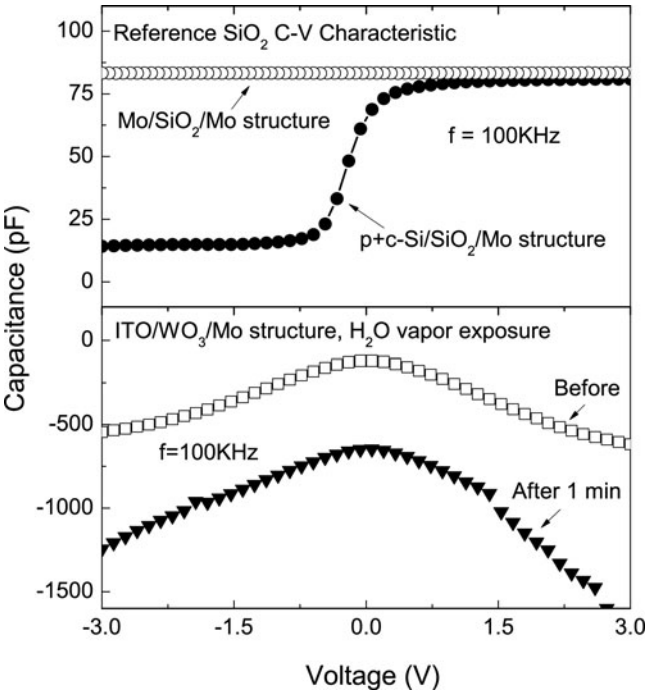

Figure 11. Capacitance (C)- voltage (V) characteristic of: (top) reference PECVD silicon dioxide thin film measured using Mo /SiO_2/p+c-Si structure and Mo/SiO_2/Mo structure at 100 kHz; (bottom) as-deposited tungsten oxide thin film and after water vapor exposure for 1 minute measured using Mo/WO_3/ITO structure at 100 kHz.

follows,

$$C_{total} = C_{H_2O} + C_{WO_3} \text{ (parallel connected)}$$

$$\frac{1}{C_{total}} = \frac{1}{C_{H_2O}} + \frac{1}{C_{WO_3}} \text{ (series connected)}$$

(*ii*) Negative capacitance may come from minority carrier injection at interface where Mo and WO_3 forms Schottky contact. As we know [28] $C = -\omega^2/L$, where ω is angular frequency and L is inductance. Negative capacitance can then be explained by inductive behavior of the device [29], where inductance behavior comes from minority carrier injection. Similar observation was made for hydrogenated amorphous silicon Schottky barrier diodes [30]. More analyses are needed to elucidate this interesting phenomenon.

3.5 Application to Electrochromic Displays

WO_3 electrochromic thin films are important for the development of ECDs, which modulates visible light transmission, glare, solar radiation and privacy while allowing views. The electrochromic rearview mirrors are already used in modern cars to glare attenuation during night driving [31] and/or to dim the airplane windows [32]. Other practical application as in architecture, vehicles, trains and aircrafts glazing [17, 33], sun glasses [34] and also to the possibility of controlling the temperature of frozen food [13] are also studied.

4. Conclusions

Thin WO_3 films were successfully prepared by the sol-gel electrogalvanostatic deposition method and were fully characterized. XRD spectra reveal amorphous nature of the films. SEM and AFM images confirmed a presence of nucleation points and a surface with 16.7 nm of RMS roughness. It was found that the films prepared by this method had reversible electrochromic properties during 3,000 chronoamperometric cycles during switching between transparent and blue color, and 61% of transmittance difference at 633 nm. From electro-optical measurements the coloration efficiency of $\eta = 11.6\ cm^2/C$ was obtained. Electrical measurements using Mo sputtered coatings show presence of negative capacitance values with the capacitance vs. potential characteristics depending on the frequency used. Based on these properties, it was found that the thin films of WO_3 showed to be very promising for applications in optical devices.

Funding

The authors are indebted to CNPq, FAPESP and CAPES, for the financial support given to this research.

References

[1] Granqvist, A. (1995). *Handbook of Inorganic Electrochromic Materials,* Elsevier Science.
[2] Monk, P. M. S., Mortimer, R.J., & Rosseinsky, D. R. (2007). *Electrochromism and Electrochromic Devices*, Cambridge University Press, New York.
[3] Granqvist, C. G. (1992). Electrochromism and Smart Window Design, *Solid State Ionics*, *53*, 479–489.
[4] Pawlicka, A., Sentanin, F., Firmino, A., Grote, J. G., Kajzar, F., & Rau, I. (2011). Ionically conducting DNA-based membranes for eletrochromic devices, *Synth. Met.*, *161/21–22*, 2329–2334.
[5] Granqvist, C. G. (2003). Solar energy materials, *Adv. Mater.*, *15/21*, 1789–1803.
[6] Hemberg, A., Konstantinidis, S., Viville, P., Renaux, F., Dauchot, J. P., Llobet, E., & Snyders, R. (2012). Effect of the thickness of reactively sputtered WO3 submicron thin films used for NO2 detection, *Sensors and Actuators B-Chemical*, *171*, 18–24.
[7] Sone, B. T., Sithole, J., Bucher, R., Mlondo, S. N., Ramontja, J., Ray, S. S., Iwuoha, E., & Maaza, M. (2012). Synthesis and structural characterization of tungsten trioxide nanoplatelet-containing thin films prepared by Aqueous Chemical Growth, *Thin Solid Films*, *522*, 164–170.
[8] da Cruz, J.S., Fraga, M. A., Braun, S., & Appel, L. G. (2007). Thermal spreading of WO3 onto zirconia support, *Applied Surface Science*, *253/6*, 3160–3167.
[9] Ai, M.(1977). Activity of Wo3-Based Mixed-Oxide Catalysts .1. Acidic Properties of Wo3-Based Catalysts and Correlation with Catalytic Activity, *Journal of Catalysis*, *49/3*, 305–312.
[10] Brinker, C. J., & Sherer, G. W. (1990). *Sol-Gel Science: The Physics and Chemistry of Sol-Gel Processing*, Academic Press Inc., San Diego, CA.
[11] Deepa, M., Srivastava, A. K., Singh, S., & Agnihotry, S. A. (2004). Structure-property correlation of nanostructured WO3 thin films produced by electrodeposition, *J. Mat. Res.*, *19/9*, 2576–2585.
[12] Deepa, M., Kar, M., & Agnihotry, S. A. (2004). Electrodeposited tungsten oxide films: annealing effects on structure and electrochromic performance, *Thin Solid Films*, *468/1-2*, 32–42.
[13] Meulenkamp, E. A. (1997). Mechanism of WO3 electrodeposition from peroxy-tungstate solution, *J. Electrochem. Soc.*, *144/5*, 1664–1671.
[14] Munro, B., Conrad, P., Kramer, S., Schmidt, H., & Zapp, P. (1998). Development of electrochromic cells by the sol-gel process, *Sol. Energ. Mat. Sol. Cells*, *54/1-4*, 131–137.

[15] Yamanaka, K. (1987). Electrodeposited Films from Aqueous Tungstic Acid-Hydrogen Peroxide Solutions for Electrochromic Display Devices, *Japanese Journal of Applied Physics Part 1-Regular Papers Short Notes & Review Papers 26/11*, 1884–1890.

[16] Bueno, P. R., Ferreira, F. F., Gimenez-Romero, D., Setti, G. O., Faria, R. C., Gabrielli, C., Perrot, H., Garcia-Jareno, J. J., & Vicente, F. (2008). Synchrotron structural characterization of electrochemically synthesized hexacyanoferrates containing K(+): A revisited analysis of electrochemical redox, *J. Phys. Chem. C*, *112/34*, 13264–13271.

[17] Heusing, S., & Aegerter, M. A., (2012). in: M. Aparicio, A. Jitianu, L. C. Klein (Eds.), *Sol-Gel Processing for Conventional and Alternative Energy*, Springer US: Boston, MA, p. 239–274.

[18] Deepa, M., Srivastava, A. K., Sharma, S. N., & Shivaprasad, S. M. (2008). Microstructural and electrochromic properties of tungsten oxide thin films produced by surfactant mediated electrodeposition, *Applied Surface Science*, *254/8*, 2342–2352.

[19] Orel, B., Krasovec, U. O., Macek, M., Svegl, F., & Stangar, U. L. (1999). Comparative studies of "all sol-gel" electrochromic devices with optically passive counter-electrode films, ormolyte Li+ ionconductor and WO3 or Nb2O5 electrochromic films, *Sol. Energ. Mat. Sol. Cells*, *56/3–4*, 343–373.

[20] Kalagi, S. S., Mali, S. S., Dalavi, D. S., Inamdar, A. I., Im, H., & Patil, P. S. (2012). Transmission attenuation and chromic contrast characterization of R.F. sputtered WO3 thin films for electrochromic device applications, *Electrochimica Acta*, *85/0*, 501–508.

[21] Cronin, J. P., Tarico, D. J., Tonazzi, J. C. L., Agrawal, A., & Kennedy, S. R. (1993). Microstructure and Properties of Sol-Gel Deposited Wo3 Coatings for Large-Area Electrochromic Windows, *Sol. Energ. Mat. Sol. Cells*, *29/4*, 371–386.

[22] Kudo, T. (1984). A New Heteropolyacid with Carbon as a Heteroatom in a Keggin-Like Structure, *Nature*, *312/5994*, 537–538.

[23] Detorresi, S. I. C., Gorenstein, A., Torresi, R. M., & Vazquez, M. V. (1991). Electrochromism of WO3 in acid acid-solutions- an electrochemical, optical and electrogravimetric study, *J. Electroanal. Chem.*, *318/1-2*, 131–144.

[24] Lee, S. H., Cheong, H. M., Tracy, C. E., Mascarenhas, A., Czanderna, A. W., & Deb, S. K. (1999). Electrochromic coloration efficiency of a-WO3-y thin films as a function of oxygen deficiency, *Appl. Phys. Lett. 75/11*, 1541–1543.

[25] Hoel, A., Kish, L. B., Vajtai, R., Niklasson, G. A., Granqvist, C. G., & Olsson, E. (2000). Electrical properties of nanocrystalline tungsten trioxide, *Nanophase and Nanocomposite Materials Iii*, *581*, 15–20.

[26] Ceiler, M. F., Kohl, P. A., & Bidstrup, S. A. (1995) Plasma-Enhanced Chemical-Vapor-Deposition of Silicon Dioxide Deposited at Low-Temperatures, *J. Electrochem. Soc.*, *142/6*, 2067–2071.

[27] Sun, D., Heusing, S., & Aegerter, M. A. (2007). Li(+) ion exchange in CeO(2)-TiO(2) sol-gel layers studied by electrochemical quartz crystal microbalance, *Sol. Energ. Mat. Sol. Cells*, *91/12*, 1037–1050.

[28] Tadros-Morgane, R., Vizdrik, G., Martin, B., & Kliem, H. (2011). Observation of negative capacitances in Al/P(VDF-TrFE)/SiO2/nSi structures, *J. Appl. Phys.*, *109*, 014501.

[29] Ershov, M., Liu, H. C., Li, L., Buchanan, M., Wasilewski, Z. R., & Jonscher, A. K. (1998). Negative capacitance effect in semiconductor devices, *IEEE Transactions on Electron Devices*, *45/10*, 2196–2206.

[30] Kanicki, J. (1985) in: D. Adler, A. Madan, M.J. Thompson (Eds.), *Mat. Res. Soc. Symp. Proc.*, Cambridge University Press, Symposium F – Materials Issues in Applications of Amorphous Silicon Technology p. 101–109.

[31] Gentext, http://www.gentex.com/automotive/mirror-module, accessed on 11/06/2013.

[32] Gentex, http://www.gentex.com/aerospace/aerospace-overview, accessed on 11/06/2013.

[33] Lampert, C. M., Agrawal, A., Baertlien, C., & Nagai, J. (1999) Durability evaluation of electrochromic devices - an industry perspective, *Sol. Energ. Mat. Sol. Cells*, *56/3-4*, 449–463.

[34] Murph, D. http://www.engadget.com/2007/03/28/electrochromic-sunglasses-change-color-on-demand/, accessed on 05/02/2014.